Kinematics of Dragonfly (*Sympetrum flaveolum*) Flight

Y.H. Chen [1], Y. Zhao [2], and W.M. Huang and D.W. Shu [1]

[1] School of Mechanical and Aerospace Engineering, Nanyang Technological University, Singapore
[2] College of Engineering, Alfaisal University, Kingdom of Saudi Arabia

***Abstract*— The kinematics of the flapping flight of the dragonfly *Sympetrum flaveolum* is investigated. The flapping patterns of the hindwing are recorded and studied thoroughly using a high speed video camera with the highest shuttle speed and resolution as reported so far on study of insect flights. The overall results indicate that the flapping pattern of a dragonfly hindwing at the nodus and the pterostigma can be either a simple figure-eight or a double figure-eight. Though the simple figure-eight trajectory is similar to that previously observed, the double figure-eight flapping trajectory is a new discovery. The angle of attack and the wing attitude are studied quantitatively. The relative position of the leading edge and trailing edge implies the presence of lift-enhancing mechanisms after stroke reversal. It is also found that the spanwise leading edge spar of a dragonfly wing is not one rigid piece, but two pieces hinged at the nodus with physical constraint of forty degrees. The elastic modulus of the costa of a hindwing is estimated through vibration tests using a vibrometer. The elastic modulus of the sampled costa from a freshly killed dragonfly is found to be in the range of rubber with small strain.**

***Keywords*— dragonfly, kinematics, flapping trajectory, trailing edge movement, nodus mobility**.

I. Introduction

Dragonflies fly in a highly manoeuvrable manner. They are capable of developing fast forward flight, hovering and backward flight. A small-scale air vehicle with such flight capabilities can be used in various applications, including military reconnaissance, search, rescue and so on. In order to mimic the effective dragonfly flight, the bionic model has to be built with similar structural mechanisms and material properties, incorporating with the actual flapping trajectories. Past research mostly focused on the study of aerodynamic lift production on insect wings. However, recent studies demonstrated that wing deformation and twisting plays an important role in boosting lift and power economy (Walker et al., 2009a; Young et al., 2009). Thus, a detailed study of wing kinematics of dragonflies are critical and necessary in understanding the aerodynamics of dragonfly flight, which in turn facilitates the simulation and design of micro-air-vehicles (MAVs).

In this paper, wing kinematics of the dragonfly, yellow-winged darter *Sympetrum flaveolum*, will be studied. In order to maintain the high shuttle speed and resolution of the recording, only the hindwing of the dragonfly will be recorded and analysed thoroughly for the flapping patterns. Analysis of critical points on the hindwing will be performed. The relative movement of each point will be digitised and recorded thus the flapping trajectories of the critical points in the hindwing can be plotted. In general, a hindwing has larger posterior wing area than a forewing. A study on the hindwing gives clearer indication of the relative trailing edge movement. Moreover, changes in hindwing motion may have more effect on changes in the aerodynamic output of the wings than that of the forewing as suggested by Wakeling and Ellington (1997). In addition, the elastic modulus of the costa of the hindwing will be studied for the material properties. Since the costa is the thickest and main supporting structure on the dragonfly wing, its rigidity has higher importance than other supporting veins.

II. Experiments and Results

A. Insects

The insect used for the experiment was the dragonfly yellow-winged darter *Sympetrum flaveolum*. The dragonflies were caught alive near Nanyang Lake in Nanyang Technological University, Singapore.

B. Conventional terminologies

Fig. 1 illustrates detailed wing morphology and conventional terminologies used in studies of dragonfly wings and thus our studies. The inserted figures were taken by the scanning electronic microscope (SEM) Leica S360. Due to the non-conductive nature of dragonfly wings, they were coated with 6 nm thickness of gold before viewing by SEM.

As noted in Fig. 1c, most of the supporting veins have needle-like micro-structures called spines on their basal and ventral sides. The spines on the basal side are shorter and blunter, while the ones on the ventral side are longer and acuter. The pterostigma is a pigmented spot near

the wing tip with a greater mass than an equally large wing piece in adjacent wing regions (Norberg, 1972). It is illustrated in Fig. 1d that the texture of the pterostigma is very different from the other membranes. It is thicker and denser than the surrounding membranes.

The anterior median vein (*MA*) shown in Fig. 1 is one important flexion line. Its function is said to help and localise the deformation of the wing during flapping, allowing alteration of camber at different stages of a flapping cycle

C. Filming of dragonfly flight

The flapping motion of the hindwings of the sampled dragonfly was captured with high speed camera and studied in detail. Before filming, four critical points (*O*, *N*, *P* and *T*) as shown in Fig. 1 were identified on the hindwing, where *O* is at the wing root, *N* is at the nodus, *P* is at the middle of the pterostigma and *T* is at the intersection of the anterior median vein (*MA*) and the trailing edge of the hindwing. These four points were chosen as the tracking points for the flapping trajectories because of their visibility on the transparent wing.

Photron high speed video camera Fastcam X-1024 PCI was used in the experiment to capture and record the flapping motion of a tethered dragonfly. Caution was exercised when calibrating the high speed camera to ensure the focus plane (at the lens) was parallel to the insect body plane (Clarke et al., 1998). The high speed video camera was calibrated every time before use and was controlled by the computer program Photron Fastcam Viewer. The high speed camera was set to 6000 frames per second (fps) with a resolution of 256 × 512 pixels, which is the highest shuttle speed and best resolution known in literature so far for study of dragonfly flights.

D. Elastic modulus of the costa

In order to obtain the elastic modulus of the costa of a dragonfly hindwing, its natural frequency was determined first via vibration test. By using Polytec scanning vibrometer (PSV) as detector and the Mini-shaker 4810 as external exciter, the natural frequency of a cantilevered costa was examined.

III. ANALYSIS AND DISCUSSION ON KINEMATICS

A. Coordinate system

The four tracking points were viewed in a global two-dimensional (2-D) coordinate system first, and then converted into a local body-centred three-dimensional (3-D) coordinate system. The films of the flapping wing were 2-D images taken from a single viewing direction by placing the camera lens parallel to the dragonfly body plane. These images were digitised in a global *x*-*y* coordinate system with both the *x* and *y* axes parallel to the filming plane. The *x* axis is horizontal and the *y* axis is vertical as shown in Fig. 2. The local body-centred 3-D coordinate system was established from the global 2-D coordinate system as illustrated in Fig. 3. When the wing flaps, its orientation keeps changing with respect to the filming plane, so that the projected lengths of *ON*, *NP* and *OT* change accordingly. During one wing-beat cycle, the wing passes through a position where it is parallel to the filming plane and gives the maximum projected wing length (Wakeling and Ellington, 1997). The maximum projected wing length captured in a film image represents scale multiples of the actual wing length, and that position should be considered as the reference plane (Ellington, 1984).

Since the origin of the local body-centred 3-D coordinate system is at the wing root, the digitised global *x*-*y* coordinates are adjusted into the new local body-centred *X*-*Y* coordinates by zeroing at the wing root point *O*. Therefore, only *Z* coordinates are unknown for the new local body-centred 3-D coordinate system. Considering the relative rigidity of the leading edge and the anterior median vein, it is reasonable to assume with high precision that the lengths of *ON*, *NP* and *OT* do not change noticeably during flapping. Hence, the corresponding orientation of the hindwing at points *N*, *P* and *T* can be calculated from the known maximum projected length and the digitised *X* and *Y* coordinates as:

$$Length = \sqrt{(X_2 - X_1)^2 + (Y_2 - Y_1)^2 + (Z_2 - Z_1)^2}$$

(1) where the subscripts 1 and 2 represent *O* and *N* respectively when calculating the length *ON*; *N* and *P* when dealing with *NP*; and, *O* and *T* when calculating *OT*. Thus the value of the *Z* coordinates can be evaluated, whereas the direction of *Z* is determined by careful observation from the film. Generally, any wing position below the reference plane was defined as positive, and above as negative.

B. Flapping trajectories at nodus and pterostigma

The motion in top view is studied using the corresponding software, Photron Motion Tools, with a sequential frame analysis. Five wing-beat cycles are analysed in detail. For the typical flapping trajectories at nodus and pterostigma, three out of five cycles demonstrate simple figure-eight trajectories at the nodus and the pterostigma (Fig. 4a for one typical result). However, the other two cycles depict a double figure-eight flapping trajectory (Fig. 4b for one typical result). No matter it is simple figure-eight or double

figure-eight, both the nodus and the pterostigma always have the same type of flapping trajectory.

C. Flapping trajectory at the trailing edge

To our best knowledge, studies of the trailing edge flapping pattern have never been reported before, although it is critical to know how the trailing edge moves in order to reproduce the insect flight accurately. Moreover, deformation of the wing can be interpreted to certain extent by studying the trailing edge movement. One surprising result is that the chosen tracking point *T* at the intersection of the anterior median vein (*MA*) and trailing edge actually shows appreciable periodic pattern. In Fig. 5, two cycles of the trajectory of point *T* are plotted. Some have suggested that *MA* is the rigid support of the posterior area of the wing judged by the relative thickness of the veins (Wootton, 1981; Wootton et al., 1998). However, no quantitative conclusions have been drawn. In our study, an appreciable flapping trajectory strongly suggests that *MA* is the supporting structure of the posterior wing. It seems only possible to have such complicated yet repeated flapping trajectory of point *T* if it has high rigidity and actively controlled at the wing root. Otherwise, it will be fluttering randomly rather than having a periodic pattern. In addition, there is no clear correlation between the occurrence of simple or double figure-eight trajectories and the production of the little loop at supinations.

D. Angle of attack with respect to time

For flapping flight of the tethered dragonfly, the angle of attack generally remains constant or changes gradually during the middle portion of upstroke and downstroke, while rapid change of angle of attack occurs during pronation and supination. Since the angle of attack is greatest near the wing root and decreases towards the wing tip, a representative of the angle of attack is drawn at 60 % wing length. This position is chosen because it is where the critical point *T* located at the intersection of *MA* and trailing edge. Thus, the angle of attack can be calculated quantitatively with the acquired kinematic data of the nodus, the pterostigma and the point *T*. Fig. 5 illustrates the angle of attack and wing attitude at 60 % wing length with respect to time course. A plot of the angle of attack versus time for five stroke cycles is shown in Fig. 5a. Red solid line shows the mean angle of attack at 60 % wing length in five flapping cycles. Grey and blue vertical lines indicate the time instants of our interests. The grey lines are numbered from 1 to 30, highlighting the time instants chosen for illustration of wing attitude during the stroke cycles. They are generally chosen at peaks and troughs of the angle of attack graph plus one temporal equidistant point in between each pair of peak and trough. The blue lines are labelled as P_i and S_i (i = 1, 2, …, 10). There are five pairs of P and S denoting the pronations and supinations respectively, and should be interpreted in pairs. Each pair of P or S starts with a smaller number denoting the onset and the following number denoting the end of the rotation. For instance, P_1 and P_2 together denote the first pronation in the sequence, with P_1 announce the onset and P_2 the end, whereas S_1 and S_2 together signify the first supination in the sequence, with S_1 the onset and S_2 the end. Moreover, wing attitude is depicted at the corresponding time instants (1-30, $P_{1\text{-}10}$, and $S_{1\text{-}9}$) indicated in Fig. 5b. Black solid lines represent the wing attitude at 60 % wing length with black solid dots marking the leading edge. The wing rotates through a relatively moderate angle during pronations and supinations as compared with the large angle of 110° observed by Ellington (1984) in various hovering insects. Typically the change in angle of attack is more pronounced in pronations, which gives rise to an average angular change of 38^o whereas it is 36^o for supinations. In general, there are two distinct patterns of wing attitude for one flapping cycle. First, pronation shows a large change in the angle of attack during wing rotation, approximately 50°, followed by supination showing another large angular change around 50°. Second, in the following flapping cycle, both the angular changes during pronation and supination reduce significantly to an average of 22°. For the five flapping cycles analysed, these two patterns occur alternatively, and the wing attitude from P_5 to P_9 is an exact repetition of that from P_1 to P_5. Thus, the trailing edge develops a periodic pattern that is twice the duration of the wing-beat cycle. This is probably the reason why trailing edge trajectory is hardly recognised before when most analysis focused on one wing-beat cycle.

The hypothesis of wake capture described by Dickinson (1994 and 1999) provides us with the necessary wing attitude for a lift-enhancing mechanism related to wing rotation. If such lift-enhancing mechanism is present, the angle of attack after stroke reversal will decrease in the forward direction of the wing motion. From the relative position of the leading edge and trailing edge shown in Fig. 5c, the angle of attack after stroke reversal reduces for all the rotations. Hence, it is reasonable to confirm that there is a lift-enhancing mechanism during wing rotation to cause a force peak after stroke reversal.

In addition, both pronation and supination are indicated with very rapid rotation through a large angle of attack in a few milliseconds, whereas the angle of attack remains constant or changes gradually during the middle portion of each half-stroke. Generally, the angle of attack remains constant during the middle portion of each half-stroke. However, the downstroke between P_4-S_3 and P_8-S_7 illustrates significant changes in the angle of attack during

the middle portion of the half-stroke. The angle of attack at the end of the pronation decreases gradually but significantly until the middle of the downstroke then increases gradually back to approximately the initial value. It is likely the lift-enhancing mechanism is still developing after stroke reversal and starts weakening at the middle portion of the downstroke. Since this phenomenon only occurs after a small angular change during pronations, it is highly possible that the strength of the lift-enhancing mechanism is related to the degree of angular acceleration during wing rotation. The cause of this lift-enhancing mechanism is still unclear at this stage. Fluid structure interaction (FSI) study should help us interpret the cause of the force peak, whether it is wake capture or wing rotational acceleration.

E. Bending of the leading edge spar

By taking three tracking points at the leading edge, deformation on the leading edge can be investigated. Fig. 6 demonstrates how angle *ONP* formed at the nodus of the hindwing changes with time as well as that of the distance from the wing root to the pterostigma *OP*. Both the angle *ONP* and distance *OP* change with time, which strongly suggests that the leading edge spar is not a rigid one piece. As shown in Fig. 1b, the angle *ONP* is slightly bending forward even at its resting position, so that the smallest value of the angle corresponds to the leading edge position when it bends most forward. Three flapping cycles are shown in Fig. 12. Both smallest values of the angle *ONP* and distance *OP* correspond to the onset of pronation, while the largest and almost constant values correspond to the supination period.

Referring to the SEM image of the nodus shown in Fig. 1b, the nodus appears to be a hinge-like structure with an L-shaped stopper. The nodus was suspected as a hinge by Sudo without in-flight experimental results to support it (Sudo et al., 1999). The study of angle *ONP* demonstrated in Fig. 6 indicates that the angle *ONP* changes over a range of 40^{o}, which will probably cause buckling failure of the costa if it is a rigid one piece. However, if the nodus is a hinge with an L-shaped stopper to restrain its freedom of rotation to approximately 40^{o}, together with any inertial-elastic and aerodynamic forces acting on the wing, the bending and rotation of the wing during pronation and supination can be well controlled. Hence, the leading edge spar of the dragonfly wing is not one rigid piece but two pieces hinged at the nodus with approximately 40^{o} freedom of rotation. We can assume that this should be applicable to forewing as well.

F. Wing profile flexion

Morphological studies of the dragonfly wings have shown that the wing is slightly cambered ventrally when it is at rest (Ennos, 1988; Ennos, 1995). Thus, it is commonly presumed that the rotation of the wing during pronation is much more difficult than that of the supination since the wing is ventrally cambered. However, study of the angle of attack shown in Fig. 5 demonstrates that the change in the angle of attack is slightly more pronounced in pronations than in supinations. Study of the angle *ONP* helps us validate the genuineness of such presumption. Referring to Fig. 7, the leading edge of the hindwing bends most forward and starts rotating at the onset of pronation. Hence, the pleated wing surface is stretched and flattened most at this point of time. By bending the costa forward and flattening the wing, it eases the wing rotation during pronations. Thus, it is a common misunderstanding that the wing rotation during pronation is much more difficult than that during supination.

IV. CONCLUSIONS

Kinematic studies of the dragonfly flight show that the flapping pattern of a dragonfly hindwing at the nodus and the pterostigma is either a simple figure-eight or a double figure-eight. The double figure-eight flapping trajectory has not been observed in in-flight experiments of dragonflies, while the simple figure-eight trajectory is similar to that reported by Wakeling and Ellington (1997). A comparison of the simple figure-eight trajectories between Wakeling and Ellington's free flight and our tethered flight shows the effect and reliability of tethered flights. It is concluded that the tethered flight conditions are not necessarily unnatural, and studies of tethered dragonfly flights which is practically much easier are as good as that of free flights in terms of kinematic measurements. Moreover, the point *T* at the intersection of *MA* and the trailing edge possesses a surprisingly periodic flapping pattern of a simple figure-eight with crossing at the middle.

The angle of attack at 60 % wing length where the critical point *T* located at the intersection of *MA* and trailing edge is drawn as a representative to show the wing attitude during the flapping cycles. The angle of attack is calculated quantitatively with the acquired kinematic data rather than estimated visually. In general, there are two distinct patterns of wing attitude for one flapping cycle. For the five flapping cycles analysed, these two patterns occur alternatively, and the pattern of wing attitude repeats after two wing-beat cycles. Thus, the trailing edge develops a periodic pattern that is twice the duration of the wing-beat cycle.

Generally, the angle of attack remains constant during the middle portion of each half-stroke. However, the downstroke after a small angular change in pronation illustrates gradual but significant decrease in the angle of attack until the middle of the downstroke then gradual increase back to approximately the initial value. It is highly possible that the strength of the lift-enhancing mechanism is related to the degree of angular acceleration during wing rotation.

The angle *ONP* formed at the nodus is not a constant. This indicates that the spanwise leading edge spar of a dragonfly hindwing is not one rigid piece, rather two pieces hinged at the nodus with physical constraint. At the nodus, the leading edges from the basal and distal wing sections are able to move relatively, but only approximately forty degrees of rotation are allowed. Therefore the dragonfly wings are unable to fold as much as that of cockroaches (Haas, 1996). On the other hand, the leading edge of the hindwing bends most forward and starts rotating at the onset of pronation, hereby eases the wing rotation during pronations. Thus, it is a common misunderstanding that the wing rotation during pronation is much more difficult than that during supination. Furthermore, the origin of torsion wave might be better explained by energy study.

Additionally, the elastic modulus of the costa of a hindwing is estimated through vibration tests. The elastic modulus of costa is found to be in the range of rubber with small strain.

References

1. **Clarke, T. A., Fryer, J. G. and Wang, X.** (1998). The Principal Point and CCD Cameras. *Photogrammetric Record* **16**, 293-312.
2. **Dickinson, M. H.** (1994). The Effects of Wing Rotation on Unsteady Aerodynamic Performance at Low Reynolds Numbers. *J. Exp. Biol.* **192**, 179-206.
3. **Dickinson, M. H., Lehmann, F.-O. and Sane, S. P.** (1999). Wing Rotation and the Aerodynamic Basis of Insect Flight. *Science* **284**, 1954-1960.
4. **Ellington, C. P.** (1984). The Aerodynamics of Hovering Insect Flight. III. Kinematics. *Phil. Trans. R. Soc. Lond. B* **305**, 41-78.
5. **Ennos, A. R.** (1988a). The Importance of Torsion in the Design of Insect Wings. *J. Exp. Biol.* **140**, 137-160.
6. **Ennos, A. R.** (1988b). The Inertial Cause of Wing Rotation in Diptera. *J. Exp. Biol.* **140**, 161-169.
7. **Ennos, A. R.** (1995). Mechanical Behaviour in Torsion of Insect Wings, Blades of Grass and Other Cambered Structures. *Proc. R. Soc. B* **259**, 15-18.
8. **Haas, F., and Wootton, R. J.** (1996). Two Basic Mechanisms in Insect Wing Folding. *Proc. R. Soc. B* **263**, 1651-1658.
9. **Norberg, R. A.** (1972). The Pterostigma of Insect Wings an Inertial Regulator of Wing Pitch. *J. Comp. Physiol.* **81**, 9-22.
10. **Sudo, S., Tsuyuki, K., Ikohagi, T., Ohta, F., Shida, S. and Tani, J.** (1999). A Study on the Wing Structure and Flapping Behavior of Dragonfly. *JSME Int Journal. Ser C. Mech Systems, Mach Elem Manuf* **42**, 721-729.
11. **Wakeling, J. M. and Ellington, C. P.** (1997). Dragonfly Flight. Ii. Velocities, Accelerations and Kinematics of Flapping Flight. *J. Exp. Biol.* **200**, 557-582.
12. **Walker, S. M., Thomas, A. L. R. and Taylor, G. K.** (2009a). Photogrammetric reconstruction of high-resolution surface topographies and deformable wing kinematics of tethered locusts and free-flying hoverflies. *J. R. Soc. Interface* **6**, 351-366.
13. **Wootton, R. J.** (1981). Support and Deformability in Insect Wings. *J. Zool.* **193**, 447-468.
14. **Wootton, R. J., Kukalová-Peck, J., Newman, D. J. S. and Muzón, J.** (1998). Smart Engineering in the Mid-Carboniferous: How Well Could Palaeozoic Dragonflies Fly? *Science* **282**, 749-751.
15. **Young, J., Walker, S. M., Bomphrey, R. J., Taylor, G. K. and Thomas, A. L. R.** (2009). Details of Insect Wing Design and Deformation Enhance Aerodynamic Function and Flight Efficiency. *Science* **325**, 1549-1552.

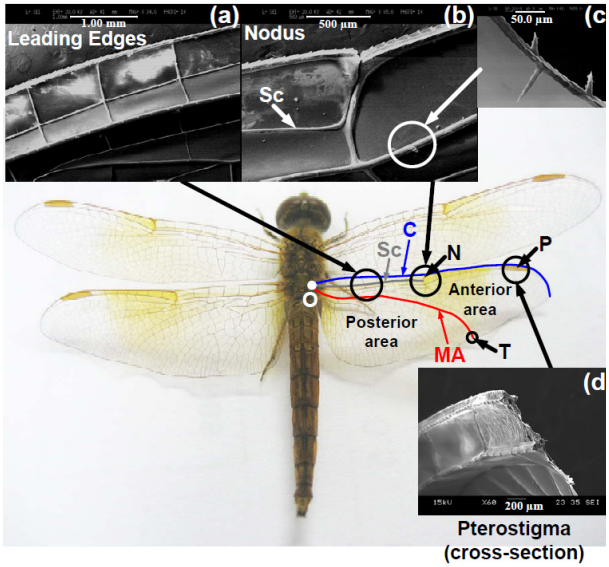

Figure 1: Detailed wing morphology and conventional terminologies used in studies of dragonfly wings.

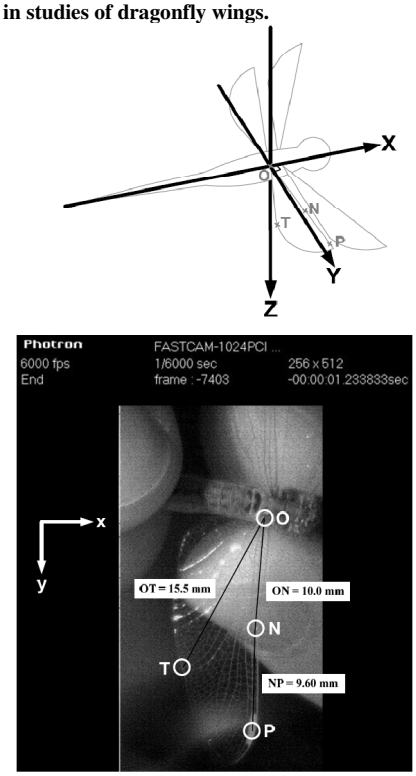

Figure 2: The filmed image of the dragonfly hindwing with critical tracking points *O*, *N*, *P* and *T*, where *O* is at the wing root, *N* is at the nodus, *P* is at the middle of the pterostigma and *T* is at the intersection of the anterior median vein (*MA*) and the trailing edge of the hindwing. The local body-centred coordinate system shown on the dragonfly hindwing.

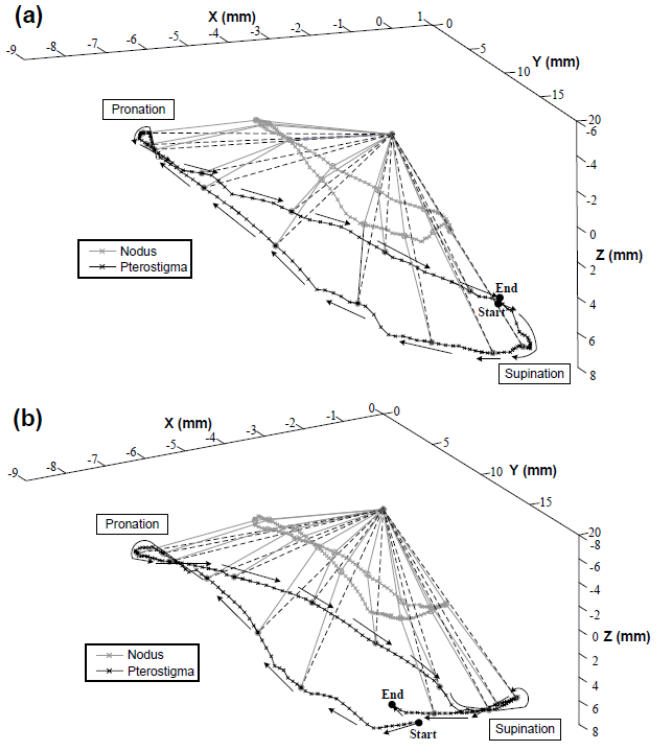

Figure 3: Typical flapping trajectories at the nodus and the pterostigma. The red broken lines connect the wing root to the pterostigma, while the blue solid lines connect the wing root to the nodus and the pterostigma at the same time instant. (a) Simple figure-eight flapping trajectories. (b) Double figure-eight flapping trajectories.

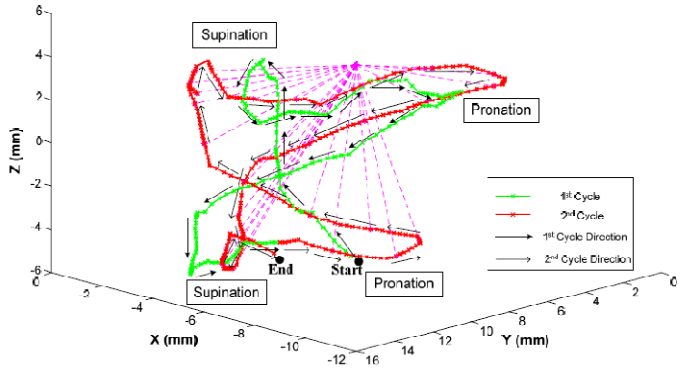

Figure 4: Two cycles of trajectory of point T at the intersection of MA and trailing edge, which the first cycle is shown in green and second cycle in red. The pink broken lines are connecting the wing root to the point T at temporal equidistance.

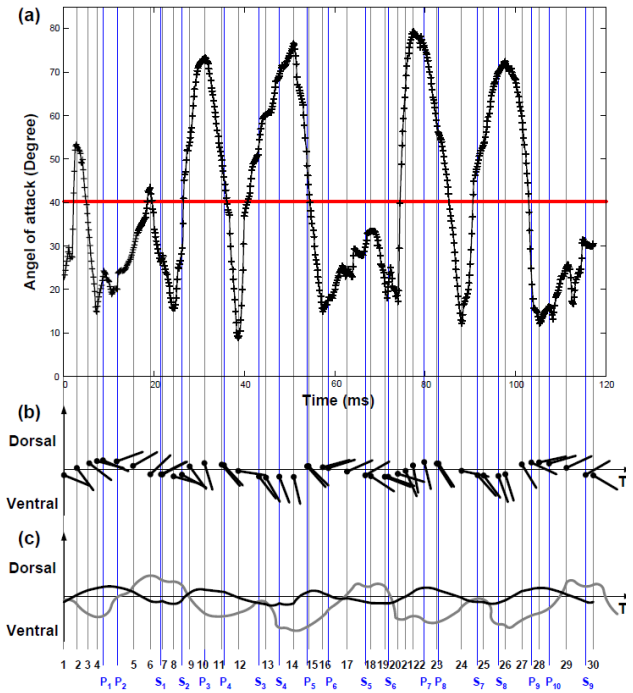

Figure 5: Angle of attack and wing attitude at 60 % wing length with respect to time. (a) Angle of attack versus time for five stroke cycles. Red solid line shows the mean angle of attack at 60 % wing length five flapping cycles. Numbered lines 1-30 highlight certain time instants during five stroke cycles, for illustration of wing attitude in time. (b) Wing attitude corresponding to time instants (1-30, $P_{1\text{-}10}$, and $S_{1\text{-}9}$) indicated. Black solid lines depict the wing attitude at 0.6*R* with black solid dots marking the leading edge. (c) The relative position of the leading edge and the trailing edge is traced according to that shown in (b). The black line shows the leading edge while the grey line the trailing edge.

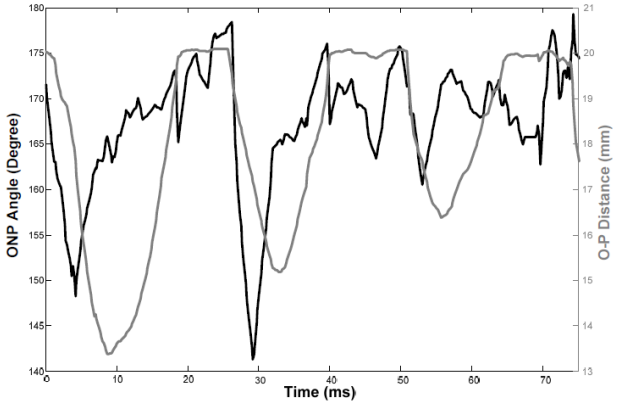

Figure 6: Changes of angle *ONP* and distance *OP* with respect to time.